Effect of phosphodiesterase 7 (PDE7) inhibitors in experimental autoimmune encephalomyelitis mice. Discovery of a new chemically diverse family of compounds

Miriam Redondo,[a] José Brea,[b] Daniel I. Perez,[a] Ignacio Soteras,[a] Cristina Val,[b] Concepción Perez,[a] Jose A. Morales-García,[c,e] Sandra Alonso-Gil,[c,e] Nuria Paul-Fernandez,[d,e] Rocío Martin-Alvarez,[d,e] María Isabel Cadavid,[b] María Isabel Loza,[b] Ana Perez-Castillo,[c,e] Guadalupe Mengod,[d,e] Nuria E. Campillo,[a] Ana Martinez,[a] Carmen Gil[a,*]

[a]Instituto de Química Médica (CSIC), Juan de la Cierva 3, 28006, Madrid (Spain)

[b]Instituto de Farmacia Industrial, Facultad de Farmacia, Universidad de Santiago de Compostela, Campus Universitario Sur s/n, 15782 Santiago de Compostela (Spain)

[c]Instituto de Investigaciones Biomédicas (CSIC-UAM), Arturo Duperier 4, 28029, Madrid (Spain)

[d]Instituto de Investigaciones Biomédicas de Barcelona (CSIC-IDIBAPS), Rosselló 161, 08036 Barcelona (Spain)

[e]Centro de Investigación Biomédica en Red sobre Enfermedades Neurodegenerativas (CIBERNED)

[*] To whom correspondence should be addressed: C. Gil, Phone: +34 91 5622900. Fax: +34 91 5644853. E-mail: cgil@iqm.csic.es

ABSTRACT: Phosphodiesterase (PDE) 7 is involved in pro-inflammatory processes being widely expressed both on lymphocytes and on certain brain regions. Specific inhibitors of PDE7 have been recently reported as potential new drugs for the treatment of neurological disorders due to their ability to increase intracellular levels of cAMP and thus, modulating the inflammatory process, as a neuroprotective well-established strategy. Multiple sclerosis is an unmet disease in which pathologies on inmunitary system, T-cells, and specific neural cells are involved simultaneously. Therefore, PDE7 inhibitors able to interfere with all these targets may represent an innovative therapy for this pathology.

Here, we report a new chemically diverse family of heterocyclic PDE7 inhibitors, discovered and optimized by using molecular modeling studies, able to increase cAMP levels in cells, decrease inflammatory activation on primary neural cultures and also attenuate the clinical symptoms in the experimental autoimmune encephalomyelitis (EAE) mouse model. These results led us to propose the use of PDE7 inhibitors as innovative therapeutic agents for the treatment of multiple sclerosis.

Keywords: PDE7 inhibitors, multiple sclerosis, drug design, docking studies

Abbreviations: ADME, Absorption, Distribution, Metabolism and Excretion; BBB, blood-brain barrier; cAMP, cyclic adenosine 3',5'-monophosphate; CFA, complete Freund's adjuvant; cGMP, cyclic guanosine 3',5'-monophosphate; CNS, central nervous system; DCC, *N*,*N*'-dicyclohexylcarbodiimide; DMEM, Dulbecco's modified Eagle's medium; DMSO, dimethyl sulfoxide; EAE, experimental autoimmune encephalomyelitis; EDTA, ethylenediaminetetraacetic acid; ES, electrospray; FBS, fetal

bovine serum; FP, fluorescence polarisation; GFAP, glial fibrillary acidic protein; GM-CSF, granulocyte-macrophage colony-stimulating factor; HAMS, Ham's F-12 nutrient mixture; HBSS, Hank's balanced salt solution; IC_{50}, inhibitory concentration 50; IMAP, Immobilized Metal Ion Affinity-Based Fluorescence Polarization, MOG, myelin oligodendrocyte glycoprotein; mRNA, messenger ribonucleic acid; MS, mass spectrometry; MTT, 3-[4, 5-dimethylthiazol-2-yl]-2, 5-diphenyltetrazolium bromide; NMR, Nuclear magnetic resonance; LPS, lipopolysaccharide; PAMPA, parallel artificial membrane permeability assay; PBL, porcine polar brain lipid; PBS, Phosphate Buffer Saline; PDEs, phosphodiesterases; PDVF, polyvinylidene difluouride; PyBOP, benzotriazol-1-yl-oxytripyrrolidinophosphonium hexafluorophosphate; SAR, structure biological activity relationships; SD, standard deviation; SDS, sodium dodecyl sulfate; SPA, Scintillation Proximity Assay; TEA, triethylamine; THF, tetrahydrofuran; UV, ultra-violet light.

INTRODUCTION

The nucleotides cyclic adenosine 3',5'-monophosphate (cAMP) and cyclic guanosine 3',5'-monophosphate (cGMP) are two ubiquitous second messengers that mediate a variety of cellular responses. Two enzymatic processes control the intracellular levels of these nucleotides: the first one by regulation of their synthesis, achieved through the action of adenylate or guanylate cyclase, and the second one through their hydrolysis catalyzed by phosphodiesterases (PDEs).[1] Up to now there are 11 known families of PDEs that control the levels of cAMP and cGMP by catalyzing their hydrolysis to AMP or GMP, respectively. The family members are classified according to their sequence identity, cellular distribution, substrate specificity, and sensitivity to different PDE inhibitors,[2, 3] being good targets for pharmacological intervention. In fact, one of the greatest advances in the PDE field in the last 15 years has been the increased availability and more recently the clinical use of family-selective inhibitors.[4] Therefore, PDE inhibitors may have considerable therapeutic utility as anti-inflammatory agents, antiasthmatics, vasodilators, smooth muscle relaxants, cardiotonic agents, antidepressants, antithrombotics, and agents for improving memory and other cognitive functions.[5] The members of the PDE superfamily are well placed to be targets for pharmacological intervention. As elevation of intracellular cAMP level shows immunosuppressive and anti-inflammatory properties,[1, 6] selective inhibitors of cAMP-specific PDEs have been widely studied as therapeutic agents for the treatment of human diseases.[5] The PDEs responsible for controlling specifically the intracellular levels of this nucleotide are PDE4, PDE7 and PDE8. More information is known about PDE4 being involved in the hydrolysis of cAMP within immune and central nervous system (CNS) cells. Thus, PDE4 inhibitors have been widely studied as efficient anti-inflammatory agents for different diseases.[7] However, a major drawback of these

compounds is the significant emetic effects. To overcome these adverse effects, several strategies have been developed.[8] An alternative approach is to target different cAMP specific PDEs families as PDE7[9] expressed also in T-cells and CNS and being a good target for the control of neuroinflammation.[10]

The PDE7 family is composed of two genes, PDE7A and PDE7B. High mRNA concentrations of both PDE7A and PDE7B are expressed in rat brain and in numerous peripheral tissues, although the distribution of these enzymes at the protein levels has not been reported. Within the brain PDE7A mRNA is abundant in the olfactory bulb, hippocampus, and several brain-stem nuclei.[11] The highest concentrations of PDE7B transcripts in the brain are found in the cerebellum, dentate gyrus of the hippocampus and striatum.[12, 13] There is very little information regarding the physiological functions regulated by PDE7. It has been shown that PDE7 is involved in pro-inflammatory processes and is necessary for the induction of T-cell proliferation.[14] Specific inhibitors of PDE7 have been recently reported as potential new drugs for the treatment of neurological disorders[15] by modulation of the inflammation process, a well-established neuroprotective strategy. Moreover, multiple sclerosis involved simultaneously pathologies on inmunitary system, T-cells, and specific neural cells, such as microglia and oligodendrocytes. Current pharmacological treatments for multiple sclerosis have severe drawbacks such as lack of efficacy and pharmacokinetics properties, being the search for new treatments and attractive field of research. PDE7 inhibitors may represent a well targeted and innovative therapy for this pathology.

Several years ago, our research group was the first one in reporting the first PDE7 selective inhibitors.[16] Since then, a lot of efforts have been done to increase potency and selectivity of this kind of compounds, conforming a great variety of diverse chemical compounds with interesting pharmacological profiles.[17]

Following our on-going research on this field, we have recently demonstrated that PDE7 inhibitors belonging to the quinazoline family enhance neuroprotection and decrease neuroinflammation in well-characterized cellular and animal models of Parkinson's disease,[18] spinal cord injury,[19] and stroke.[20]

With the aim to design potent and specific PDE7 inhibitors, we developed a pharmacophore model for PDE7A1 inhibitors using Catalyst/Hypogen program to identify the chemical features that are responsible for the inhibitory activity.[21] Four pharmacophore features, such as one hydrogen bond acceptor, one aromatic ring and two hydrophobic aliphatic points were identified to be involved in inhibitor-PDE7 interaction (Chart 1). This pharmacophore model was able to predict the activity of external test set of PDE7 inhibitors with a correlation coefficient of 0.96. New leads identification was carried out by performing virtual screening using validated pharmacophoric queries and four chemical databases (Maybridge, Chemical Diversity, Specs and National Cancer Institute). Further data reduction was done employing virtual filters based on distances (T=1.5Å), angles (10º) and Lipinski's rules of five. According to this procedure, three new hits (**1**-**3**) were found as potential PDE7A1 inhibitors structurally diverse from those previously known[22] (Table 1). Then, the biological activity of the hits was calculated using the catalytic domain of PDE7A1 and a radiometric assay.

Here, Chart 1

Here, Table 1

These three hits were selected for further medicinal chemistry programs aimed to increase not only efficacy but also the ADME profile to be considered for further drug development in the neurodegenerative field. Here, the results obtained in the development of the family derived from the furan **1** and its therapeutic potential for multiple sclerosis are reported.

RESULTS AND DISCUSSION

Chemistry. The 5-(2-methyl-4-nitrophenyl)-2-furylmethyl 3,4,5-triethoxybenzoate (**1**) has a furan heterocycle between two substituted phenyl rings moieties. In particular, the structural modifications proposed are based on the modification of the number and nature of substituents attached to both phenyl rings and the variation of the linker between the furan and the alkyloxyphenyl ring (Chart 2).

Here, Chart 2

The synthetic routes for the preparation of the furan derivatives are summarized in Schemes 1 and 2. The 5-phenyl-2-furylmethyl benzoate derivatives (Scheme 1) were obtained in one synthetic step, after the coupling reaction of the alkyloxybenzoic acid and the corresponding 5-phenyl-2-furylmethanol. These furan alcohols were commercial available with the only exception of 5-(2,4-dichlorophenyl)-2-furylmethanol (**4**) which was synthesized by reduction of the 5-(2,4-dichlorophenyl)-2-furoic acid with lithium aluminum hydride as described in the supporting information.

Here, Scheme 1

The synthesis of benzyl 5-phenylfuroate and benzyl 5-phenylfuramide derivatives (Scheme 2) involved the coupling of alkyloxybenzyl alcohol or alkyloxybenzyl amine with the furoic acid derivative. Among different coupling reagents previously used, benzotriazol-1-yl-oxytripyrrolidinophosphonium hexafluorophosphate (PyBOP) was chosen as the most convenient one.

The structures of all the synthesized products were unequivocally confirmed by mass spectrometry, elemental analysis, and ^{1}H and ^{13}C NMR spectroscopic data.

Here, Scheme 2

***In vitro* evaluation of PDE7 inhibition.** The new derivatives here synthetized (**5-32**) were tested for their inhibitory potencies against PDE7A1 using recombinant human isoenzyme as described in the experimental section. All the compounds were tested at a fixed concentration (10 μM) by duplicate. The percentage of inhibition obtained on PDE7A1 for all the compounds at this concentration is showed in Table 2. From these data we can conclude that several new compounds are inhibitors of PDE7A1.

Here, Table 2

As the biological assay conditions differs from that previously used,[22] the lead compound **1** was also here evaluated to compare the data with the new synthesized derivatives. Noteworthy is the fact that when the lead compound **1** was evaluated in the new experimental conditions using the complete enzyme instead of the catalytic domain of PDE7A1, only a 29% of PDE7A1 inhibition at 10 μM was found. Regarding this

new data, modifications performed on the chemical structure of **1** increase in general the inhibition of PDE7A1.

When the percentage of PDE7A1 inhibition was greater than 50%, the dose response curve was determined and the IC_{50} values calculated (Table 3). Some of these new compounds present IC_{50} values regarding PDE7A1 inhibition in the low micromolar range being suitable candidates to be further explored. A kinetic study varying cAMP concentration was performed with two of these compounds (**13** and **31**) to better characterize the enzymatic inhibition. Double-reciprocal plotting of the data is depicted in figure 1. The intercept of the plot in the horizontal axis (1/[cAMP]) changes when the compound **13** and **31** concentrations increase, whereas the intercept in the vertical axis (1/V) does not change. These results suggest that furan derivatives act as competitive inhibitors of cAMP binding site and allow us to determine the Ki of these inhibitors, (5.91 and 7.22) for compounds **13** and **31** respectively.

Here, Table 3

Here, Figure 1

Docking studies. In order to gain some insight in the binding mode of our family of compounds, docking experiments were carried out with help of Surflex method implemented in Sybyl according to the procedure described in the experimental section. Considering the kinetic studies results, the docking studies were focused on the cAMP binding site. After careful examination of docking solutions two binding modes that can draw the chemical structure biological activity relationships (SAR) in this serie of compounds were proposed. In fact, the different substituents and their location (*ortho*, *meta* or *para*) when R^3 is a phenyl ring, determine which binding mode is selected.

The mainly binding mode (namely "A" from now) is characterized by a hydrophobic interaction of the phenyl group in R^3 with Val380 and a NH-π interaction[23, 24] with Gln413, which is in fact, a conserved residue among PDEs families.[25] A clearly example of this binding mode is compound **13** (see figure 2). In addition to these interactions, the furan moiety contributes to increase inhibition by means of a stacking interaction with another conserved residue as Phe416. Furthermore, the 3,4,5-trimethoxy-phenyl ligand's moiety is located in a pocket where the ligand can take benefit of a hydrogen bond between the methoxy group in R^2 and the proton H_ε of His256 group ($d_{H\varepsilon...O}$ = 2.7Å) and a hydrophobic interaction with Phe384.

Here, Figure 2

When R^1 and R^2 are ethoxy groups (compound **24**), the binding mode remains mode "A", (see figure 3). The presence of these bigger substituents forces the ligand to reorient the ester group keeping a hydrophobic interaction with Phe384. This new location causes a weakening of the parallel stacking interaction between the furan ring and Phe416 (found for compound **13**) because of the displacement of the furan ring in order to keep the hydrophobic interaction between ligand's benzene ring in R_3 and Val380. As a result, compound **24** shows a lower percentage of PDE7A1 inhibition than compound **13** (table 2).

Here, Figure 3

Regarding the substituent located in *para* position in the phenyl attached in R^3 such a methyl group (compound **23**), the ligand orients this substituent facing it towards the

Leu401 adopting thus the binding mode "B" (see figure 4). This new orientation avoids potential steric clashes and allows the establishment of a new hydrophobic interaction between the methyl group and the side chain of Leu401 meanwhile the previous stacking between the furan and Phe416 is mostly conserved. Furthermore, this new orientation forces the second phenyl ring to a new position where two new interactions with Ile323 are established which can help to stabilize the ligand in this new binding mode.

Here, Figure 4

Finally, when the ester group linker is replaced by an amide one, (compounds **30-32**), the conformation of the ligands dramatically changes by the formation of an intra-molecular hydrogen bond between NH group and furan's oxygen. This conformation allows new stabilizing interactions between the phenyl ring with Leu401's side chain where it can interact hydrophobically (Figure 5).

Here, Figure 5

***In vitro* antiinflamatory studies.** Our next step was to explore whether these new PDE7 inhibitors are able to reduce the inflammatory response in different cell based assays. Thus, we used primary cultures of astrocytes and microglia treated with lipopolysaccharide (LPS), a potent inflammatory agent.

The potential anti-inflammatory activity of the selected PDE7 inhibitors (**7**, **13**, **14**, **19** and **31**) was measured by evaluating the production of nitrites from primary cultured glial cells (astrocytes and microglia). To asses the safety of the compounds on cell

culture, the astrocytes and microglia viability were checked using the 3-[4, 5-dimethylthiazol-2-yl]-2, 5-diphenyltetrazolium bromide (MTT) test at two different concentrations of the compounds. As both concentrations used do not affect the cell survival, they were selected for the antiinflammatory experiment.

Cultures were incubated with the indicated concentrations of the compounds **7**, **13**, **14**, **19**, **21** and **31** for 1 h, and then cells were treated for 24 h with LPS. When primary astrocytes and microglial cells were stimulated with LPS (Figures 6 and 7) a significant induction of nitrite production in the culture medium, was produced, while if the PDE7 inhibitors were in the medium a significant decrease of nitrite production was observed as a consequence of a reduction of the inflamatory cell response by the drug treatment. We used as standard references the well known PDE4 inhibitor Rolipram and the PDE7 inhibitor BRL50481.[26] These compounds showed a neuroprotective effect which was in accordance with our previously reported results,[20] confirming that these cell permeable PDE7 inhibitors are able to decrease neural inflammatory activation.

Here, Figure 6

Here, Figure 7

Candidate selection for *in vivo* studies. The final aim of our study was to proof the potential efficacy of these new PDE7 inhibitors in a multiple sclerosis murine model. The selection of the candidate for *in vivo* studies was done based on pharmacological and pharmacokinetic properties.

Recently, potential cardiotoxic effect of long-term PDE3A inhibition was reported.[27] Thus, to avoid adverse effects in further development steps we measured the inhibition on PDE3A of our selected compounds (Table 4).

Here, Table 4

Considering these new data, almost every derivative tested inhibit PDE3A at the same concentration that PDE7A1 was also inhibited, showing a lack of selectivity and opening safety concerns in further pharmacological development. However, derivative **13** shows an IC_{50} value tenfold higher on PDE3A regarding PDE7A1 (ratio PDE7A1/PDE3A=0.09), selecting this candidate for the next studies.

To evaluate isoenzyme specificity of **13**, inhibition of different cAMP isoenzymes was determined (Table 5). While marginal inhibition was found on PDE4B2, no activity was found on PDE7B and PDE4D3. The partial inhibition of PDE4B2 may increase the biological action of **13** *in vivo* because cAMP levels might be enhanced. Moreover, it is worth mentioning that inhibition of PDE4D3 is associated to the adverse emetic effects in the development of PDE4 inhibitors.[28] As derivative **13** does not inhibit this specific isoenzyme, its safety potential regarding PDEs inhibition is reinforced.

Here, Table 5

We also check the ability of derivative **13** to regulate intracellular cAMP levels in cell cultures. Two different compound concentrations (10 and 30 μM) were used and in both cases we observed an increase of cAMP even more effective than the reported PDE7 inhibitor BRL50481[26] (Figure 8).

Here, Figure 8

Finally, and to decipher if this compound has the drug profile to be administered *in vivo*, we determined its ability to cross the blood-brain barrier (BBB), one of the major obstacles for the treatment of diseases in the central nervous system. The majority of compounds enter the brain by transcellular passive diffusion, which is driven by a concentration gradient between the blood and the brain.[29] Parallel Artificial Membrane Permeability Assay (PAMPA) is a high throughput technique developed to predict passive permeability through biological membranes. Here, we used the PAMPA-BBB method described by Di *et al*.[30] employing a brain lipid porcine membrane, to determine the ability of compound **13** to penetrate into the brain. The *in vitro* permeabilities (*Pe*) of commercial drugs through lipid membrane extract together with compound **13**, were determined and described. A good correlation between experimental and described values *Pe* (exp)= 1.1512 (bibl) - 0.8973 (R^2= 0.9779) was obtained (see supporting information). From this equation, the *Pe* (exp) for **13** is $(8.1 \pm 0.1)10^{-6}$ cm s^{-1}. Following the pattern established in the literature for BBB permeation prediction[31] that classify compounds as CNS + when they present a permeability > 3.71 x 10^{-6} cm s^{-1}, we can consider that compound **13** is able to cross the BBB by passive permeation.

***In vivo* studies. Experimental autoimmune encephalomyelitis model.** The results found in cell cultures for the new PDE7 inhibitor **13** together with their ability to cross the BBB, prompted us to evaluate it in chronic experimental autoimmune encephalomyelitis (EAE) mice, a well establish murine model for multiple sclerosis.

EAE was induced in C57BL/6J mice by immunization with MOG_{35-55} in complete Freund's adjuvant on day 0. Clinical signs and score were monitored up to day 41. Mice

began to show neurological deficits on day 12, reaching a maximum score around day 16. A therapeutic regimen of administration was chosen to test the PDE7 inhibitor in the EAE model. Thus a daily i.p. administration of compound **13** for 26 days started at day 5 after disease onset. The dose was selected considering the IC_{50} value on the target and the cellular anti-inflammatory activity. As we can see in figure 9A, a clear and significant attenuation of clinical symptoms during the first 16 days of treatment (day 32 after immunization figure 9A) was observed. However, this behavior is lost in the last ten days of treatment. The body weight curve (Figure 9B), reflects these findings and the compound **13**-treated mice start to lose weight in the same frame-time than clinical scores decrease (described above).

This experiment showed for the first time efficacy of PDE inhibitors on a well established model of multiple sclerosis. Compound **13** administrated to the EAE when the worst neurological score was measured, showed a recovery of the clinical symptoms reaching a statistically significant plateau of maximum effect from day 21 to 31 p.i. However, this attenuation of the symptoms was counterbalanced by the worsening of the animals during the last 10 days of treatment until day 42, when the animals were sacrificed. To decipher if this effect is due to the administrated compound (stability, metabolism, etc) or to the animal model further studies are in progress.

Here, Figure 9

CONCLUSIONS

PDE7 inhibitors represent a new class of innovative drugs with great potential for several neurological disorders. Their efficacy in animal models of Parkinson disease, stroke, and spinal cord injury has been recently reported while their value for the

treatment of multiple sclerosis is here disclosed. We presented the medicinal chemistry program around one hit found by using a pharmacophore model. The work lead to a novel serie of PDE7 inhibitors, chemically diverse from those known and containing a furan ring in their chemical structure.

The biological profile has been well characterized showing an increase of cAMP level and a reduction of the inflammatory response in primary neural cell cultures. Moreover, a clear strategy to select the best compound for *in vivo* testing, using pharmacodynamic and pharmacokinetic criteria was followed. Finally, compound **13** was chosen due to its PDE7 selectivity and its ability to cross the BBB. This compound is able to reverse clinical symptoms in an EAE mice model. All together these data supported the potential of PDE7 inhibitors for the therapeutic pharmacological treatment of multiple sclerosis.

EXPERIMENTAL

Chemical procedures. Substrates were purchased from commercial sources and used without further purification. Melting points were determined with a Mettler Toledo MP70 apparatus. Flash column chromatography was carried out at medium pressure using silica gel (E. Merck, Grade 60, particle size 0.040-0.063 mm, 230-240 mesh ASTM) with the indicated solvent as eluent. Compounds were detected with UV light (254 nm). ^{1}H NMR spectra were obtained on the Bruker AVANCE-300 spectrometer working at 300 MHz or on a Varian INOVA 400 spectrometer working at 400 MHz. Typical spectral parameters: spectral width 10 ppm, pulse width 9 μs (57°), data size 32 K. ^{13}C NMR experiments were carried out on the Bruker AVANCE-300 spectrometer operating at 75 MHz or on a Varian INOVA 400 spectrometer working at 100 MHz. The acquisition parameters: spectral width 16 kHz, acquisition time 0.99 s, pulse width 9 μs (57°), data size 32 K. Chemical shifts are reported in values (ppm) relative to internal Me_4Si and *J* values are reported in Hz. Elemental analyses were performed by the analytical department at CENQUIOR (CSIC), and the results obtained were within ± 0.4% of the theoretical values.

***5-(4-Phenyl)-2-furylmethyl 3,4,5-triethoxybenzoate* (7)**. PyBOP (358 mg, 0.68 mmol) was added as coupling reagent to a solution of 3,4,5-triethoxybenzoic acid (175 mg, 0.68 mmol) with TEA (158 μL, 1.15 mmol) in CH_2Cl_2 (10 mL) followed by 5-phenyl-2-furylmethanol (100 mg, 0.57 mmol), and the resulting mixture was stirred at 25 ºC during 12 hours. The reaction mixture was evaporated *in vacuo* and the solid was purified by column cromatography on silica using hexane/ethyl acetate (8:1) as eluent to afford a yellow solid (246 mg, 87% yield). mp 71.1 ºC. ^{1}H NMR (300 MHz, $CDCl_3$): δ 7.70-7.29, 6.64, 6.56, 5.33, 4.10, 1.42, 1.35. ^{13}C NMR (75 MHz, $CDCl_3$): δ 166.5,

153.0, 149.5, 149.1, 129.2, 125.7, 128.1, 125.7, 124.3, 124.4, 113.7, 108.8, 106.3, 69.4, 65.2, 59.2, 16.0, 15.2. MS (ES, $[M+K]^+$): *m/ z* = 449. Anal. $C_{25}H_{28}O_5$ (C, H, O).

3,4,5-Trimethoxybenzyl 5-phenyl-2-furoate **(13).** PyBOP (639 mg, 1.23 mmol) was added as coupling reagent to a solution of 5-phenyl-2-furoic acid (200 mg, 1.03 mmol) with TEA (284 µL, 2.06 mmol) in CH_2Cl_2 (10 mL) followed by 3,4,5-trimethoxybenzyl alcohol (210 µL, 1.27 mmol), and the resulting mixture was stirred at 25 ºC during 23 hours. The reaction mixture was evaporated *in vacuo* and the solid was purified by column cromatography on silica using hexane/ethyl acetate (8:1) as eluent to afford a white solid (90 mg, 24% yield). mp 98.4 ºC. ^{1}H NMR (300 MHz, $CDCl_3$): δ 7.79, 7.45-7.26, 6.69, 5.29, 3.93-3.85. ^{13}C NMR (75 MHz, $CDCl_3$): δ 159.0, 158.2, 153.7, 143.9, 138.5, 131.7, 129.8, 129.4, 129.2, 125.3, 120.7, 107.3, 106.1, 67.1, 61.2, 56.6. MS (ES, $[M+Na]^+$): *m/ z* = 391. Anal. $C_{21}H_{20}O_6$ (C, H, O).

3,4,5-Trimethoxybenzyl 5-(2-trifluoromethylphenyl)-2-furoate **(14).** PyBOP (393 mg, 0.76 mmol) was added as coupling reagent to a solution of 5-(2-trifluoromethylphenyl)-2-furoic acid (200 mg, 0.76 mmol) with TEA (174 µL, 1.26 mmol) in CH_2Cl_2 (10 mL) followed by 3,4,5-trimethoxybenzyl alcohol (129 µL, 0.65 mmol), and the resulting mixture was stirred at 25 ºC during 12 hours. The reaction mixture was evaporated *in vacuo* and the solid was purified by column cromatography on silica using hexane/ethyl acetate (6:1) as eluent to afford a white solid (123 mg, 36% yield). mp 89.8 ºC. ^{1}H NMR (300 MHz, $CDCl_3$): δ 7.80, 7.68, 7.53, 7.30, 6.79, 6.69, 5.30, 3.89, 3.86. ^{13}C NMR (75 MHz, $CDCl_3$): δ 158.8, 154.5, 153.7, 144.8, 138.5, 132.3, 131.6, 131.1, 129.5, 128.8, 127.3, 124.1, 120.2, 112.4, 106.1, 67.2, 61.3, 56.5. MS (ES, $[M+Na]^+$): *m/ z* = 459. Anal. $C_{22}H_{19}F_3O_6$ (C, H, O).

3,4,5-Trimethoxybenzyl 5-(4-chloro-2-nitrophenyl)-2-furoate **(19).** PyBOP (369 mg, 0.71 mmol) was added as coupling reagent to a solution of 5-(4-chloro-2-

nitrophenyl)-2-furoic acid (200 mg, 0.71 mmol) with TEA (164 μL, 1.19 mmol) in CH_2Cl_2 (10 mL) followed by 3,4,5-trimethoxybenzyl alcohol (101 μL, 0.61 mmol), and the resulting mixture was stirred at 25 ºC during 12 hours. The reaction mixture was evaporated *in vacuo* and the solid was purified by column cromatography on silica using hexane/ethyl acetate (6:1) as eluent to afford a white solid (130 mg, 38% yield). mp 147.3 ºC. ^{1}H NMR (300 MHz, $CDCl_3$): δ 8.37-7.87, 7.86, 7.30, 5.87, 4.48, 4.44. ^{13}C NMR (75 MHz, $CDCl_3$): δ 158.5, 153.8, 151.1, 148.4, 145.6, 138.5, 136.1, 132.8, 131.4, 131.2, 124.9, 122.0, 124.8, 120.2, 112.2, 106.0, 67.4, 61.3, 56.6. MS (ES, $[M+Na]^+$): *m/ z* = 470. Anal.$C_{25}H_{28}O_5$ (C, H, O).

***3,4,5-Trimethoxybenzyl 5-(4-nitrophenyl)-2-furoate* (21).** PyBOP (509 mg, 0.98 mmol) was added as coupling reagent to a solution of 5-(4-nitrophenyl)-2-furoic acid (200 mg, 0.82 mmol) with TEA (227 μL, 1.64 mmol) in CH_2Cl_2 (10 mL) followed by 3,4,5-trimethoxybenzyl alcohol (168 μL, 0.98 mmol), and the resulting mixture was stirred at 25 ºC during 24 hours. The reaction mixture was evaporated *in vacuo* and the solid was purified by column cromatography on silica using hexane/ethyl acetate (4:1) as eluent to afford a white solid (34 mg, 10% yield). mp 161.2 ºC. ^{1}H NMR (300 MHz, $CDCl_3$): δ 7.52, 7.93, 7.31, 6.95, 6.69, 5.30, 3.93-3.86. ^{13}C NMR (75 MHz, $CDCl_3$): δ 158.6, 155.4, 153.8, 147.9, 145.6, 143.2, 135.4, 131.4, 125.7, 124.8, 120.6, 110.5, 106.3, 67.5, 61.3, 56.6. MS (ES, $[M+Na]^+$): *m/ z* = 436. Anal. $C_{21}H_{19}NO_8$ (C, H, N, O).

***3,4,5-Trimethoxybenzyl 5-(4-methyl-2-nitrophenyl)-2-furamide* (31).** PyBOP (618 mg, 1.19 mmol) was added as coupling reagent to a solution of 5-(4-methyl-2-nitrophenyl)-2-furoic acid (300 mg, 1.19 mmol) with TEA (274 μL, 1.98 mmol) in CH_2Cl_2 (10 mL) followed by 3,4,5-trimethoxybenzylamine (173 μL, 0.99 mmol), and the resulting mixture was stirred at 25 ºC during 12 hours. The reaction mixture was evaporated *in vacuo* and the solid was purified by column cromatography on silica

using hexane/ethyl acetate (3:1) as eluent to afford a yellow solid (56 mg, 14% yield). mp 114.2 ºC. ^{1}H NMR (300 MHz, $CDCl_3$): δ 7.49, 7.34, 7.15, 6.65, 6.51, 4.48, 3.81, 3.75, 2.39. ^{13}C NMR (75 MHz, $CDCl_3$): δ 158.2, 153.9, 150.6, 148.4, 148.2, 141.1, 137.3, 133.9, 133.2, 125.2, 124.8, 120.7, 116.6, 111.5, 105.1, 61.3, 56.6, 43.8, 21.5. MS (ES, $[M+H]^+$): *m/ z* = 427. Anal. $C_{22}H_{22}N_2O_7$ (C, H, N, O).

Radiometric phosphodiesterase inhibition assay. The methodology used for measuring human recombinant PDE7A1, PDE7B and PDE3A activity was based in a Scintillation Proximity Assay (SPA) from Perkin Elmer (TRKQ7090). The activity of the phosphodiesterase is measured by co-incubating the enzyme with [^{3}H]cAMP and the hydrolysis of the nucleotide is quantified by radioactivity measurement after binding of [^{3}H]AMP to scintillation binding bead.

Either 0.02 units of PDE7A1 (Calbiochem # 524751), 0.02 units of PDE3A (Calbiochem # 524742) or 0.5 units of PDE7B (Abcam # ab79800) were incubated in a 96-well flexiplate with 5 nCi of [^{3}H]cAMP and inhibitors in 100 µL of assay buffer (contained in the kit) for 20 min at 30ºC. After the incubation time, 50µL of a solution of SPA-beads (approximately 1 mg per well) were added to each well and plate was shaken for 1 hour at room temperature. Finally, beads were settled for 30 min and radioactivity was detected in a Microbeta Trilux reader.

IC_{50} values were calculated by non-linear regression fitting using GraphPad Prism. Data (radioactivity *vs* log concentration) was fitted to a sigmoidal dose-response equation: Y = Bottom + (Top-Bottom)/(1+10^((logIC_{50}-X)*n)), where Bottom and Top were the minimum and maximal inhibition for PDE, respectively, IC_{50} was the concentration of compound that inhibited the PDE activity in a 50% and n was the slope of the concentration-response curve.

The mode of inhibitory action for compound **13** and **31** was determined by varying the concentration of unlabelled cAMP in the reaction cocktail within the range of 5nM to 2μM in the presence of a fixed concentration of [^{3}H]-cAMP tracer and inhibitor concentrations. Enzyme activity data were analyzed using Lineweaver-Burk plots using GraphPad Prism.

Fluorescence polarization phosphodiesterase inhibition assay. The ability of compounds to inhibit PDE4B2 (human recombinant) and PDE4D3 (human recombinant) was determined by IMAP Fluorescence Polarisation (FP) assay (Molecular Devices R8175).

0.05U of PDE4B2 (Calbiochem # 524736), PDE4D3 (Calbiochem # 524733) were incubated in a 96-well black half-area plate with 1nM of Fluorescein adenosine 3′,5′-cyclic phosphate (contained in the kit) and inhibitors in 40μL of assay buffer. Plates were mixed on a shaker for 10 seconds and incubated at ambient temperature for 60 minutes. IMAP binding reagent was added (60 μL of a 1 in 600 dilution in binding buffer of the kit stock solution) to terminate the assay. Plates were allowed to stand at ambient temperature for 1 hour. The FP ratio was measured with a Tecan Ultra Evolution Reader.

IC_{50} values were calculated by non-linear regression fitting using GraphPad Prism. Data (fluorescence polarization *vs* log concentration) was fitted to a sigmoidal dose-response equation: Y = Bottom + (Top-Bottom)/(1+10^((logIC_{50}-X)*n)), where Bottom and Top were the minimum and maximal inhibition for PDE, respectively, IC_{50} was the concentration of compound that inhibited the PDE activity in a 50% and n was the slope of the concentration-response curve.

Molecular modeling. To carry out docking analysis, chain A of protein structures were processed with help of Sybyl8.0 software[32] adding hydrogens, and capping

terminal residues with neutral ends. Then, newly added hydrogen positions were optimized with MMFF94 force field until a 0.01kcal/mol gradient was reached. Ligand geometries were also minimized with MMFF94 force field until a 0.01kcal/mol gradient was reached.

The docking studies were performed with Surflex (Sybyl). An "Automatic" protocol was generated and dockings were carried out using 20 initial conformations for each ligand allowing flexibility. Pre and post minimization was used considering 100 solutions in each case. Cscore scoring function was used with all the four options and claiming for a relaxed structure.

Visual inspection of solutions of selected ligands was carried out in order to find which ones allow the best agreement with SAR data. Finally the selected ligand-complex geometries were minimized with MMFF94 force field until a 0.01kcal/mol gradient was reached.

To test our docking protocol and validate the procedure, we carried out docking experiments for some selected 3D structures The first one was for the complex of 3,5-dimethyl-1-(3-nitrophenyl)-1*H*-pyrazole-4-carboxylic acid ethyl ester bound to PDE4D (pdb code 1Y2K), as this ligand shares a high similarity with some of our inhibitors. The high similarity between the docked solution (only one cluster within 2.0Å rmsd of heavy atoms was found) and the experimental one gave us confidence in our protocol (rmsd 0.2Å of heavy atoms *vs* exp., see figure S2 in the supporting information). In fact, the main difference between both orientations is related with the benzene with supports a nitro group. This difference can be explained due to the lack of water W1016 from the pdb, which was not present in the model of PDE4D used for docking were only the metal coordination waters (W1003-W1008) were retained. On the other hand, in order to test our protocol specifically in PDE7, we carried out the docking experiment with

the 3D structures of pdb code 1ZKL and 3G3N. In the case of 1ZKL, the reproduction of the experimental binding mode of IBMX inhibitor was only possible (rmsd 0.1Å of heavy atoms *vs* exp., see figure S3 in the supporting information) when waters W573 and W542 were added aside with the metal coordination waters (W504-W509). This fact is not surprising as those two additional water molecules are within 3.0Å from the ligand. As only those two structures of PDE7A were available at the moment of this study (pdb codes. 1ZKL, 3G3N), and given the redocking results obtained for 3G3N we decided to use structure 1ZKL for docking purposes. Finally, as the best redocking results were obtained for structure 1Y2K, which ligand is the most similar to our inhibitors, we decided to retain only the metal coordination waters present in pdb code 1ZKL for docking.

Primary cell cultures. Glial cells were prepared from neonatal rat cerebral cortex, as previously described by Luna-Medina et al.[33] Briefly, after removal of the meninges the cerebral cortex was dissected, dissociated, and incubated with 0.25% trypsin/EDTA at 37 ºC for 1 hour. After centrifugation, the pellet was washed 3 times with HBSS (Gibco) and the cells were plated on non-coated flasks and maintained in HAMS/DMEM (1:1) medium containing 10% FBS. After 15 days the flasks were agitated on an orbital shaker for 4 hours at 240 rpm at 37 ºC, the supernatant was collected, centrifuged, and the cellular pellet containing the microglial cells resuspended in complete medium (HAMS/DMEM (1:1) containing 10% FBS) and seeded on uncoated 96-well plates. Cells were allowed to adhere for 2 hours and the medium was removed to eliminate non-adherent oligodendrocytes. New fresh medium containing 10 ng/mL of GM-CSF was added. The remaining astroglial cells adhered on the flasks were then trypsinized, collected, centrifugated and plated onto 96-well plates with complete medium. The purity of cultures obtained by this procedure was >98% as

determined by immunofluorescence with the OX42 (microglial marker) and the GFAP (astroglial marker) antibodies. After 1 week in culture, cells were treated with Rolipram, BRL50481 and the different compounds (**7**, **13**, **14**, **19**, **21** and **31**) at several concentrations. Cell viability was then measured after 16h in culture. For nitrite release quantification some cultures were also treated with lipopolysaccharide (LPS; 10µg/mL) alone or in combination with compounds.

Cell viability assay. Cell viability was measured using the MTT assay from Roche, based on the ability of viable cells to reduce yellow MTT to blue formazan. Briefly, cells cultured in 96-well plates and treated with the indicated compounds for 16h were incubated with MTT (0.5mg/mL, 4h) and subsequently solubilized in 10% SDS/0.01M HCl for 12h in the dark. The extent of reduction of MTT was quantified by absorbance measurement at 595nm according to the manufacturer´s protocol.

Nitrites measurement. Accumulation of nitrites in media was assayed by the standard Griess reaction. After stimulation of cells with the different compounds, supernatants were collected and mixed with an equal volume of Griess reagent (Sigma). Samples were then incubated at room temperature for 15 minutes and absorbance read using a plate reader at 492/540 nm.

cAMP measurements in Raw cells. Quantification of cAMP was carried out using the EIA (enzyme immunoassay) kit from GE Healthcare. Briefly, Raw cells were seeded at 3x104/well in 96-well dishes and incubated overnight before the assay. After 60 min incubation with compound **13**, cAMP intracellular levels were determined following the manufacture's instructions.

CNS penetration: *In vitro* Parallel artificial membrane permeability assay (PAMPA)-Blood brain barrier (BBB). Prediction of the brain penetration was evaluated using a parallel artificial membrane permeability assay (PAMPA).[30] Ten

commercial drugs, phosphate buffer saline solution at pH 7.4 (PBS), Ethanol and dodecane were purchased from Sigma, Acros organics, Merck, Aldrich and Fluka. The porcine polar brain lipid (PBL) (catalog no. 141101) was from Avanti Polar Lipids. The donor plate was a 96-well filtrate plate (Multiscreen® IP Sterile Plate PDVF membrane, pore size is 0.45 μM, catalog no. MAIPS4510) and the acceptor plate was an indented 96-well plate (Multiscreen®, catalog no. MAMCS9610) both from Millipore. Filter PDVF membrane units (diameter 30 mm, pore size 0.45 μm) from Symta were used to filtered the samples. A 96-well plate UV reader (Thermoscientific, Multiskan spectrum) was used for the UV measurements. Test compounds [(3-5 mg of Caffeine, Enoxacine, Hydrocortisone, Desipramine, Ofloxacine, Piroxicam, Testosterone), (12 mg of Promazine) and 25 mg of Verapamile and Atenolol] were dissolved in EtOH (1000 μL). 100 microlitres of this compound stock solution was taken and 1400 μL of EtOH and 3500 μL of PBS pH 7.4 buffer were added to reach 30% of EtOH concentration in the experiment. These solutions were filtered. The acceptor 96-well microplate was filled with 180 μL of PBS/EtOH (70/30). The donor 96-well plate was coated with 4 μL of porcine brain lipid in dodecane (20 mg mL^{-1}) and after 5 minutes, 180 μL of each compound solution was added. 1-2 mg of every compound to be determined their ability to pass the brain barrier were dissolved in 1500 μL of EtOH and 3500 μL of PBS pH 7.4 buffer, filtered and then added to the donor 96-well plate. Then the donor plate was carefully put on the acceptor plate to form a "sandwich", which was left undisturbed for 2h and 30 min at 25 °C. During this time the compounds diffused from the donor plate through the brain lipid membrane into the acceptor plate. After incubation, the donor plate was removed. UV plate reader determined the concentration of compounds and commercial drugs in the acceptor and the donor wells. Every sample was analyzed at three to five wavelengths, in 3 wells and in two independent runs. Results are given as

the mean [standard deviation (SD)] and the average of the two runs is reported. 10 quality control compounds (previously mentioned) of known BBB permeability were included in each experiment to validate the analysis set.

EAE induction and treatment. Six-week-old female C57BL6 mice (15-20 g) were purchased from Harlan (Spain). All experimental procedures followed the European Communities Council Directive of November 24, 1986 (86/609/EEC). The protocol was approved by the ethic committee of the University of Barcelona and of the Generalitat de Catalunya. The mice were maintained on a 12h light/dark cycle at a constant environmental temperature with free access to food and water for 1 week prior to experimentation.

EAE was induced by subcutaneous immunization with 100μg MOG_{35-55} peptide (EspiKem S.r.l., Italy) in 100μL complete Freund's adjuvant (CFA) (Sigma-Aldrich) enriched with *Mycobacterium tuberculosis* (H37Ra strain, Difco, Detroit, MI, USA). Mice were immediately intraperitoneally injected with 200ng of *Bordetella pertussis* toxin (Sigma-Aldrich) and again 48h after the immunization.

Animals (n=13) were weighed and examined for clinical signs on a daily basis. Disease severity of EAE was graded according to a five-point scale: Grade 0 = no disability; 1 = a flaccid tail; 2 = a mild but definite weakness of one or both hind legs; 3 = moderate paraparesis of one hind leg; 4 = no hind leg movement; 5 = a moribund state with little or no spontaneous movement and impaired respiration.[34]

Stock solution of the compound (100mg/mL in DMSO) was diluted 1:50 in a solution of 5% Tocrisolve (Tocris, UK) in distilled water. Mice were treated through daily intraperitoneal (i.p.) injection starting on day 5 after the onset of the disease at a dose of 10 mg/kg of animal (n=7) or with only vehicle (n=7).

ACKNOWLEDGEMENTS

The authors gratefully acknowledge the financial support of Ministry of Science and Innovation (MICINN), projects nos. SAF2009-13015-C02-01, SAF2009-13015-C02-02, SAF2010-16365, SAF2009-1152, and PI10-01874; Instituto de Salud Carlos III (ISCiii), project no. RD07/0060/0015 (RETICS program) and CIBERNED; Fundación Española para la Ciencia y la Tecnología (FECYT), project no. FCT-09-INC-0367. M. R. and D. I. P. acknowledge pre- and post-doctoral fellowship from the CSIC (JAE program) respectively. BRAINco Biopharma is acknowledged**.**

SUPPORTING INFORMATION

Elemental analyses of compounds **5**-**32**; experimental procedures for compounds **4**-**6**, **8**-**12**, **15**-**18**, **20**, **22**-**30** and **32**; linear correlation between experimental and described values in the PAMPA-BBB assay; figures S1 and S2. This material is available free of charge via the Internet at http://pubs.acs.org.

REFERENCES

(1) Essayan, D. M. Cyclic nucleotide phosphodiesterase (PDE) inhibitors and immunomodulation. *Biochem. Pharmacol.* **1999,** *57*, 965-973.

(2) Conti, M.; Jin, S. L. The molecular biology of cyclic nucleotide phosphodiesterases. *Prog. Nucleic Acid Res. Mol. Biol.* **1999,** *63*, 1-38.

(3) Bender, A. T.; Beavo, J. A. Cyclic nucleotide phosphodiesterases: molecular regulation to clinical use. *Pharmacol. Rev.* **2006,** *58*, 488-520.

(4) Francis, S. H.; Conti, M.; Houslay, M. D. *Phosphodiesterases as drug targets*. Springer-Verlag Berlin Heidelberg: 2011.

(5) Lugnier, C. Cyclic nucleotide phosphodiesterase (PDE) superfamily: A new target for the development of specific therapeutic agents. *Pharmacol. Ther.* **2006,** *109*, 366-398.

(6) Allison, A. C. Immunosuppressive drugs: the first 50 years and a glance forward. *Immunopharmacology* **2000,** *47*, 63-83.

(7) Houslay, M. D.; Schafer, P.; Zhang, K. Y. Keynote review: phosphodiesterase-4 as a therapeutic target. *Drug Discov. Today* **2005,** *10*, 1503-1519.

(8) Giembycz, M. A. Life after PDE4: overcoming adverse events with dual-specificity phosphodiesterase inhibitors. *Curr. Opin. Pharmacol.* **2005,** *5*, 238-244.

(9) Conti, M.; Beavo, J. Biochemistry and physiology of cyclic nucleotide phosphodiesterases: essential components in cyclic nucleotide signaling. *Annu. Rev. Biochem.* **2007,** *76*, 481-511.

(10) Giembycz, M. A.; Smith, S. J. Phosphodiesterase 7A: a new therapeutic target for alleviating chronic inflammation? *Curr. Pharm. Des.* **2006,** *12*, 3207-3220.

(11) Miro, X.; Perez-Torres, S.; Palacios, J. M.; Puigdomenech, P.; Mengod, G. Differential distribution of cAMP-specific phosphodiesterase 7A mRNA in rat brain and peripheral organs. *Synapse* **2001,** *40*, 201-214.

(12) Sasaki, T.; Kotera, J.; Omori, K. Novel alternative splice variants of rat phosphodiesterase 7B showing unique tissue-specific expression and phosphorylation. *Biochem. J.* **2002,** *361*, 211-220.

(13) Reyes-Irisarri, E.; Perez-Torres, S.; Mengod, G. Neuronal expression of cAMP-specific phosphodiesterase 7B mRNA in the rat brain. *Neuroscience* **2005,** *132*, 1173-1185.

(14) Nakata, A.; Ogawa, K.; Sasaki, T.; Koyama, N.; Wada, K.; Kotera, J.; Kikkawa, H.; Omori, K.; Kaminuma, O. Potential role of phosphodiesterase 7 in human T cell function: comparative effects of two phosphodiesterase inhibitors. *Clin. Exp. Immunol.* **2002,** *128*, 460-466.

(15) Gil, C.; Campillo, N. E.; Perez, D. I.; Martinez, A. Phosphodiesterase 7 (PDE7) inhibitors as new drugs for neurological and inflammatory disorders. *Expert Opin. Ther. Pat.* **2008,** *18*, 1127-1139.

(16) Martinez, A.; Castro, A.; Gil, C.; Miralpeix, M.; Segarra, V.; Domenech, T.; Beleta, J.; Palacios, J. M.; Ryder, H.; Miro, X.; Bonet, C.; Casacuberta, J. M.; Azorin, F.; Piña, B.; Puigdomenech, P. Benzyl derivatives of 2,1,3-benzo- and benzothieno[3,2-a]thiadiazine 2,2-dioxides: first phosphodiesterase 7 inhibitors. *J. Med. Chem.* **2000,** *43*, 683-689.

(17) Castro, A.; Jerez, M. J.; Gil, C.; Martinez, A. Cyclic nucleotide phosphodiesterases and their role in immunomodulatory responses: advances in the development of specific phosphodiesterase inhibitors. *Med. Res. Rev.* **2005,** *25*, 229-244.

(18) Morales-Garcia, J.; Redondo, M.; Gil, C.; Alonso-Gil, S.; Martinez, A.; Santos, A.; Perez-Castillo, A. Phosphodiesterase 7 inhibition preserves dopaminergic neurons in cellular and rodent models of Parkinson disease. *PLoS ONE* **2011,** *6*, e17240.

(19) Paterniti, I.; Mazzon, E.; Gil, C.; Impllizzari, D.; Palomo, V.; Redondo, M.; Perez, D. I.; Esposito, E.; Martinez, A.; Cuzzocrea, S. PDE 7 inhibitors: new potential drugs for the therapy of spinal cord injury. *PLoS ONE* **2011,** *6*, e15937.

(20) Redondo, M.; Zarruk, J. G.; Ceballos, P.; Perez, D. I.; Perez, C.; Perez-Castillo, A.; Moro, M. A.; Brea, J.; Val, C.; Cadavid, M. I.; Loza, M. I.; Campillo, N. E.; Martinez, A.; Gil, C. Neuroprotective efficacy of quinazoline type phosphodiesterase 7 inhibitors in cellular cultures and experimental stroke model. *Eur. J. Med. Chem.* **2012,** *47*, 175-185.

(21) Jerez, M. J.; Castro, A.; Gil, C.; Martinez, A. Development of a pharmacophoric model for specific PDE7 inhibitors. *Drugs Fut.* **2004,** *29 (Supp. A)*, 129.

(22) Gil, C.; Castro, A.; Jerez, M. J.; Ke, H.; Wang, H.; Ballester, S.; González-García, C.; Martínez, A. New PDE7 inhibitors leads for neurodegenerative diseases discovered by using a pharmacophoric model. *Drugs Fut.* **2008,** *33 (Supp. A)*, 228.

(23) Vaupel, S.; Brutschy, B.; Tarakeshwar, P.; Kim, K. S. Characterization of weak NH-pi intermolecular interactions of ammonia with various substituted pi-systems. *J. Am. Chem. Soc.* **2006,** *128*, 5416-5426.

(24) Mohan, N.; Vijayalakshmi, K. P.; Koga, N.; Suresh, C. H. Comparison of aromatic NH...pi, OH...pi, and CH...pi interactions of alanine using MP2, CCSD, and DFT methods. *J. Comput. Chem.* **2010,** *31*, 2874-2882.

(25) Ke, H.; Wang, H. Crystal structures of phosphodiesterases and implications on substrate specificity and inhibitor selectivity. *Curr. Top. Med. Chem.* **2007,** *7*, 391-403.

(26) Smith, S. J.; Cieslinski, L. B.; Newton, R.; Donnelly, L. E.; Fenwick, P. S.; Nicholson, A. G.; Barnes, P. J.; Barnette, M. S.; Giembycz, M. A. Discovery of BRL 50481 [3-(N,N-dimethylsulfonamido)-4-methyl-nitrobenzene], a selective inhibitor of phosphodiesterase 7: in vitro studies in human monocytes, lung macrophages, and CD8+ T-lymphocytes. *Mol. Pharmacol.* **2004,** *66*, 1679-1689.

(27) Movsesian, M. A.; Kukreja, R. C. Phosphodiesterase inhibition in heart failure. *Handb. Exp. Pharmacol.* **2011**, 237-249.

(28) Robichaud, A.; Stamatiou, P. B.; Jin, S. L.; Lachance, N.; MacDonald, D.; Laliberte, F.; Liu, S.; Huang, Z.; Conti, M.; Chan, C. C. Deletion of phosphodiesterase 4D in mice shortens alpha(2)-adrenoceptor-mediated anesthesia, a behavioral correlate of emesis. *J. Clin. Invest.* **2002,** *110*, 1045-1052.

(29) Di, L.; Kerns, E. H.; Carter, G. T. Strategies to assess blood-brain barrier penetration. *Expert Opin. Drug Discov.* **2008,** *3*, 677-687.

(30) Di, L.; Kerns, E. H.; Fan, K.; McConnell, O. J.; Carter, G. T. High throughput artificial membrane permeability assay for blood-brain barrier. *Eur. J. Med. Chem.* **2003,** *38*, 223-232.

(31) Crivori, P.; Cruciani, G.; Carrupt, P. A.; Testa, B. Predicting blood-brain barrier permeation from three-dimensional molecular structure. *J. Med. Chem.* **2000,** *43*, 2204-2216.

(32) SYBYL 8.0, Tripos International, 1699 South Hanley Rd., St. Louis, Missouri, 63144, USA.

(33) Luna-Medina, R.; Cortes-Canteli, M.; Alonso, M.; Santos, A.; Martinez, A.; Perez-Castillo, A. Regulation of inflammatory response in neural cells in vitro by thiadiazolidinones derivatives through peroxisome proliferator-activated receptor gamma activation. *J. Biol. Chem.* **2005,** *280*, 21453-21462.

(34) McFarlin, D. E.; Blank, S. E.; Kibler, R. F. Recurrent experimental allergic encephalomyelitis in the Lewis rat. *J. Immunol.* **1974,** *113*, 712-715.

TABLES

Table 1. PDE7A1 activities for derivatives **1-3**.

Compound	Chemical structure	Experimental IC_{50} PDE7A1 (μM)
1	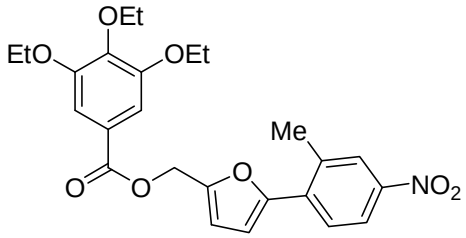	0.58±0.09[22]
2	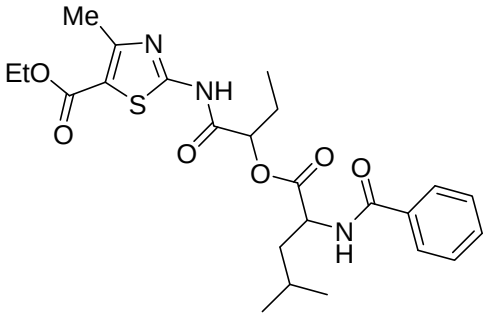	0.86±0.04[22]
3	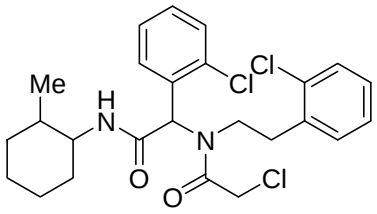	0.88±0.16[22]

Table 2. PDE7A1 inhibition of compounds (**5-32**).

Comp.	%inh PDE7A1 @10μM	Comp.	%inh PDE7A1 @10μM
5	24.4 ±13.4	**19**	49.1±9.5
6	49.5 ±3.0	**20**	14.0±1.1
7	48.8 ±11.1	**21**	48.0 ±7.7
8	3.7 ± 2.0	**22**	14.0±7.8
9	39.9 ±8.6	**23**	30.7±14.8
10	16.4 ± 1.1	**24**	30.8±0.5
11	10.0±6.9	**25**	31.1±8.7
12	-9.9±1.5	**26**	29.2 ±0.2
13	57.9±0.1	**27**	28.0±4.5
14	54.9±3.6	**28**	44.8±1.2
15	34.6±2.3	**29**	41.6±6.5
16	38.3±7.8	**30**	23.5±0.4
17	8.0±0.1	**31**	70.5±4.6
18	28.8±0.2	**32**	-10.3±0.6

Table 3. IC_{50} values for PDE7A1 of selected compounds and BRL50481 as standard reference.[a]

Comp.	**6**	**7**	**13**	**14**	**19**	**21**	**31**
PDE7A1 IC_{50} (μM)	33.37±8.1	12.34±3.22	5.17±1.11	2.63± 0.92	7.31±3.57	14.07±2.9	3.20±1.23

[a]IC_{50} (BRL50481) = 0.09 μM

Table 4. PDE3A inhibition for selected compounds.

Comp.	%inh PDE3A @10μM	IC_{50} PDE3A (μM)	Ratio PDE7A1 /PDE3A
7	3.0±12.7	104.2±36.6	0.12
13	46.1±3.0	54.6±12.1	0.09
14	74.9±5.4	1.8±0.85	1.44
19	11.0±4	n.d.	n.d.
21	57.1±12	3.4±1.3	4.15
31	49.6±1.2	3.9±0.7	0.82

Table 5. IC_{50} values (μM) on different PDEs for compound **13**.

Comp.	PDE7A1	PDE7B	PDE3A	PDE4B2	PDE4D3
13	5.1±1.11	23.2±4.4%@10μM	54.6±8.1	12.4±4.2	66.3±13.9

FIGURES

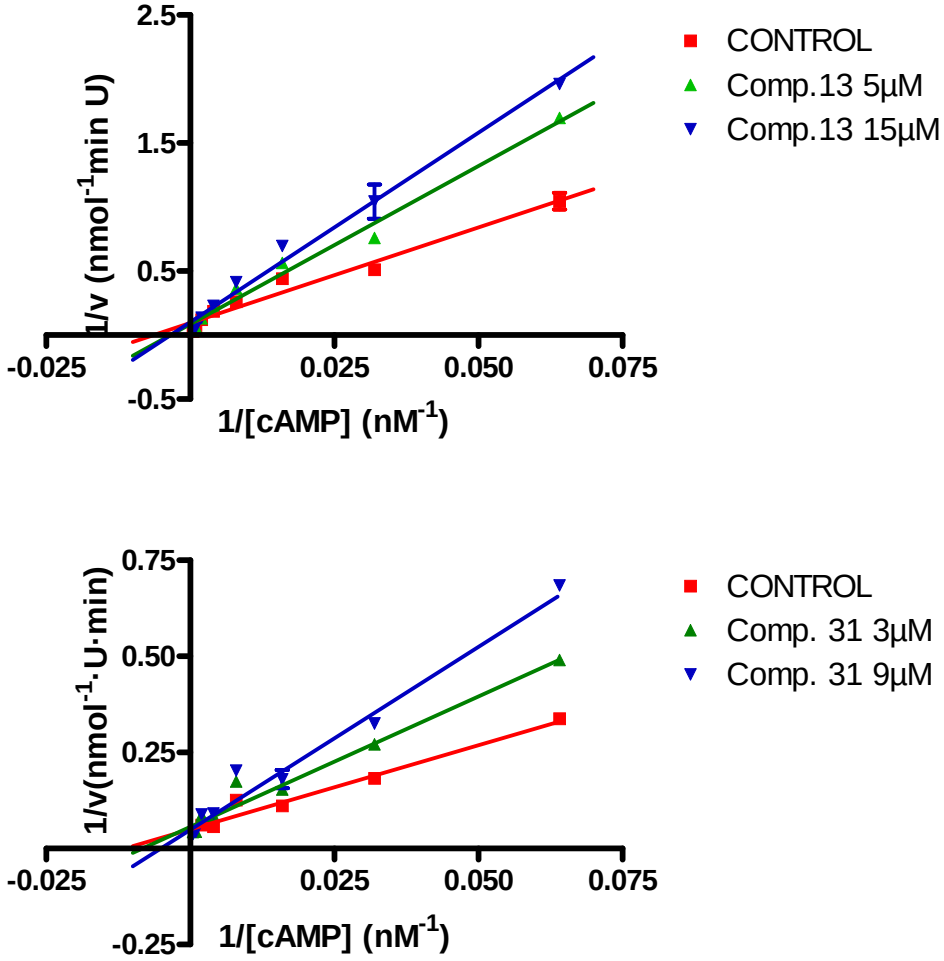

Figure 1. Studies of the PDE7A1 inhibition in the absence (control) and in the presence of two different concentrations of the furan derivatives **13** and **31** incubating different cAMP concentrations and measuring AMP formation. Data represent the mean±sem (vertical bars) of triplicate measurements.

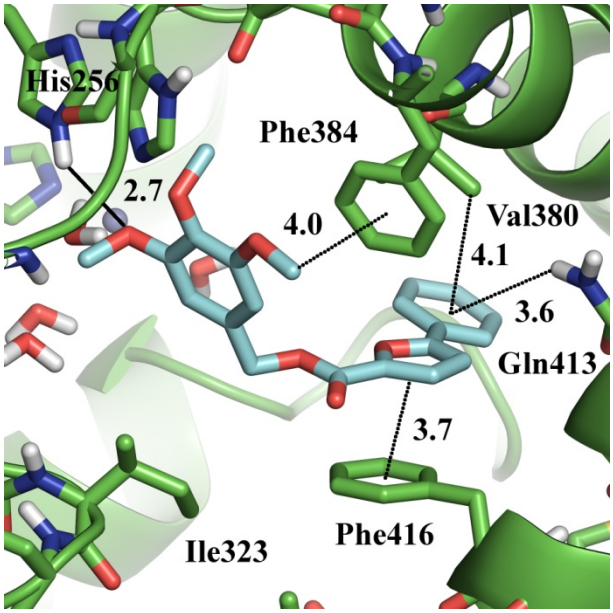

Figure 2. Proposed binding mode for compound **13** (pdb code 1ZKL) showing relevant interactions with nearby residues. Distances are given in angstroms.

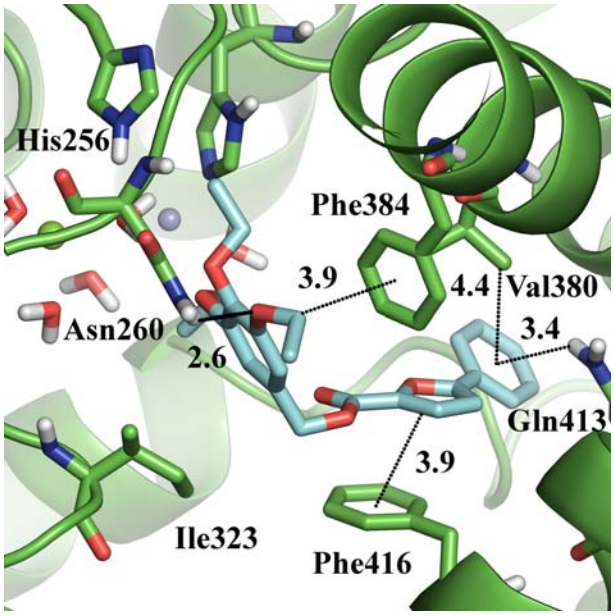

Figure 3. Proposed binding mode for compound **24** (for pdb code 1ZKL) showing relevant interactions with nearby residues. Distances are given in angstroms.

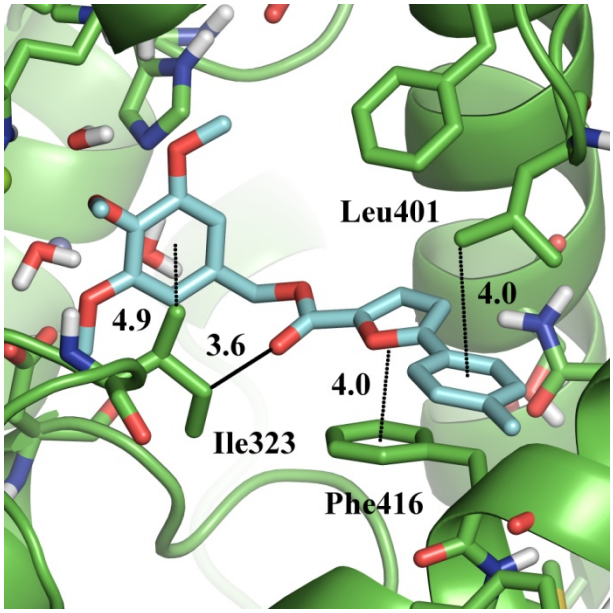

Figure 4. Proposed binding mode for compound **23** (pdb code 1ZKL) showing relevant interactions with nearby residues. Distances are given in angstroms.

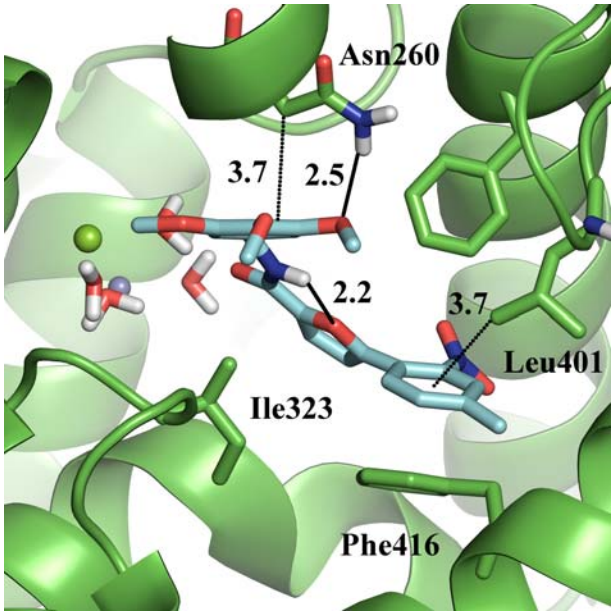

Figure 5. Proposed binding mode for compound **31** (pdb code 1ZKL) showing relevant interactions with nearby residues. Distances in angstroms.

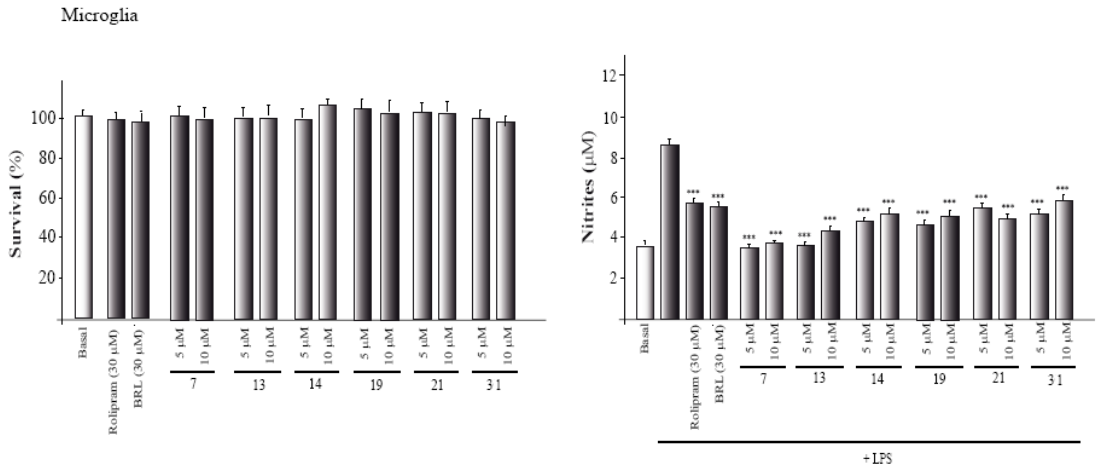

Figure 6. Cell viability and nitrite production. Glial cultures were treated during 16h with Rolipram (30 μM), BRL50481 (BRL; 30 μM) and compounds **7**, **13**, **14**, **19**, **21**, **31** (5 or 10 μM) and cell viability measured. Some cultures were treated with lipopolysaccharide (LPS), in presence or absence of compound at indicated concentrations, and the production of nitrites measured as indicated in the experimental section. Values represent the mean ± SD of six replications in three different experiments. *** $p<0.001$ *versus* LPS-treated cells.

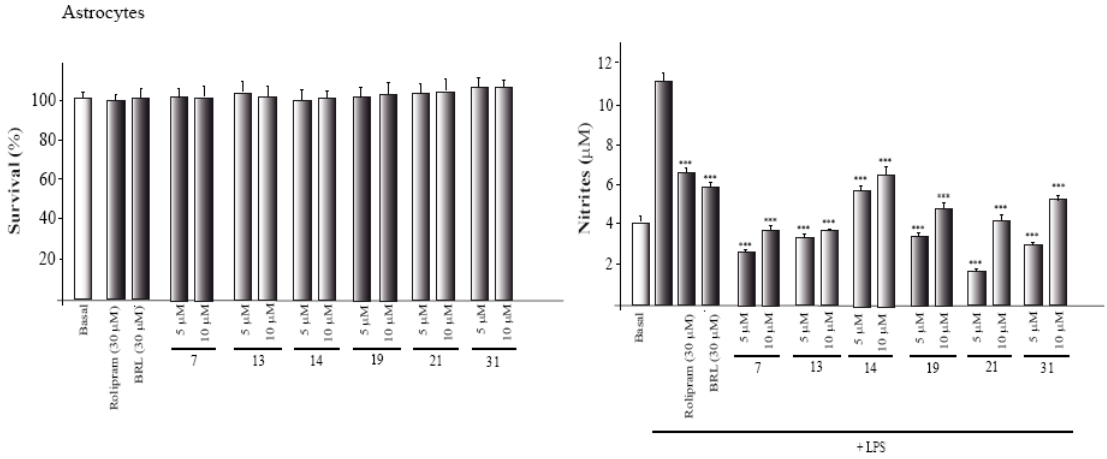

Figure 7. Cell viability and nitrite production. Astrocytes cultures were treated during 16h with Rolipram (30 µM), BRL50481 (BRL; 30 µM) and compounds **7**, **13**, **14**, **19**, **21**, **31** (5 or 10 µM) and cell viability measured. Some cultures were treated with lipopolysaccharide (LPS) in presence or absence of compound at indicated concentrations, and the production of nitrites measured as indicated in the experimental section. Values represent the mean ± SD of six replications in three different experiments. *** $p<0.001$ *versus* LPS-treated cells.

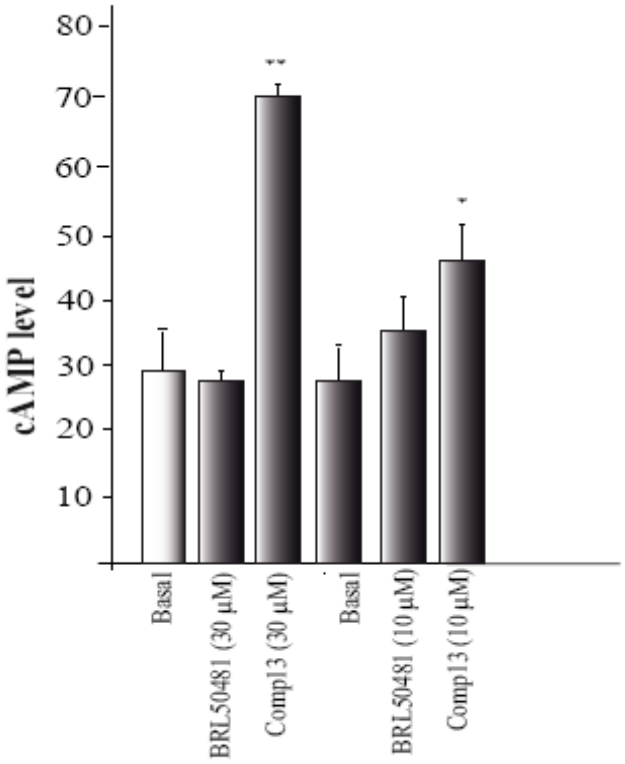

Figure 8. Intracellular cAMP level in Raw cells treated with compound **13** at 30 and 10 μM.

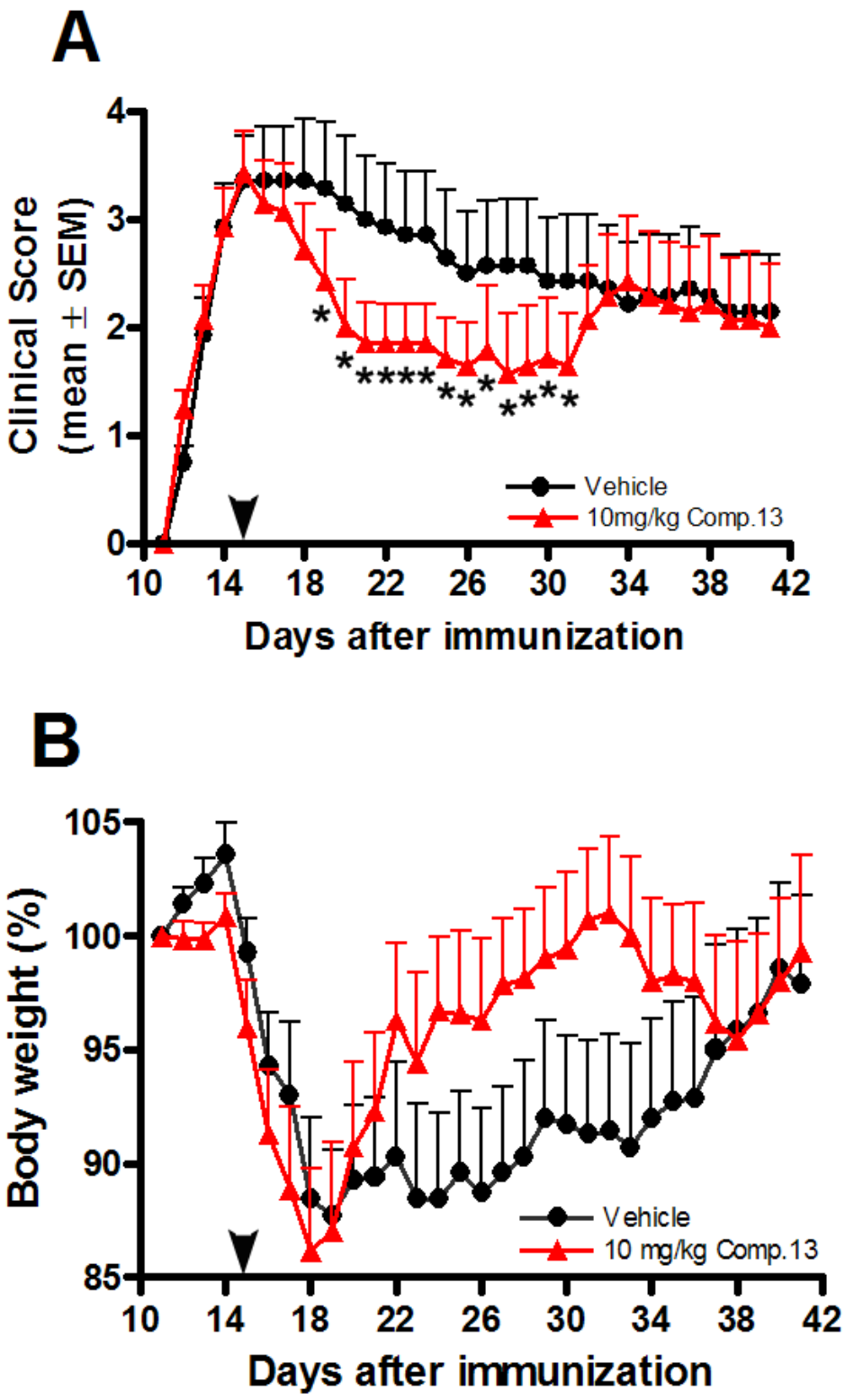

Figure 9. Therapeutic effect of compound **13** in MOG35-55-induced EAE in C57BL6J mice. Fourteen C57BL6J mice immunized with MOG35-55 at 100 µg /mouse in the

presence of complete Freund's adjuvant developed clinical signs on day 12. Animals were divided into two groups. One group was treated with compound **13** starting from day 5 after the onset of the disease (arrowhead) for 26 days. Mice in the control group were administered vehicle only. A) EAE scores in drug treatment; B) percentage of body weight variation. Results were expressed as the mean ± standard error of the mean and statistical differences in EAE scores between the vehicle and the treatment group was calculated by Mann-Whitney test (*$p<0.0002$). **●,** Vehicle (n=7)**; ▲,** 10 mg/kg compound **13** (n=7) i.p. daily.

SCHEMES

Scheme 1[a]

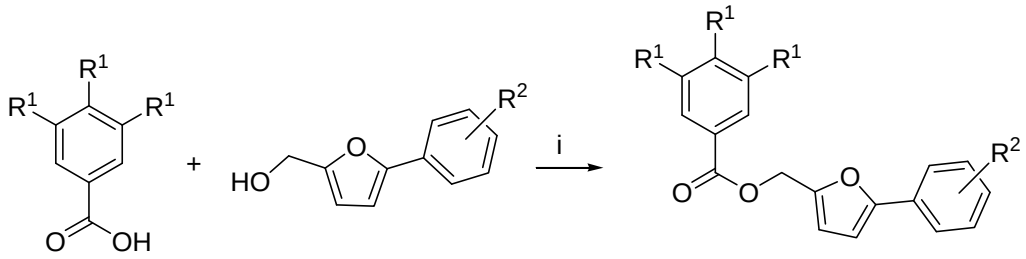

R^1 = OMe	R^2 = 2,4-diCl	**5**
	R^2 = 4-NO_2	**6**
R^1 = OEt	R^2 = H	**7**
	R^2 = 2,4-diCl	**8**
	R^2 = 4-NO_2	**9**
	R^2 = 4-Me	**10**

[a]Reagents: i) Coupling reagent, TEA, r.t., CH_2Cl_2

Scheme 2[a]

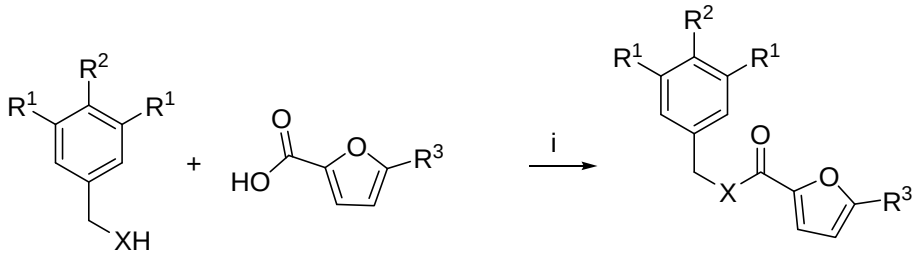

X=O, R^1=R^2 = OMe	R^3 = H	**11**
	R^3 = Me	**12**
	R^3 = Ph	**13**
	R^3 = 2-CF_3-Ph	**14**
	R^3 = 2-Cl-Ph	**15**
	R^3 = 2,4-diCl-Ph	**16**
	R^3 = 2-Cl, 5-CF_3-Ph	**17**
	R^3 = 2-NO_2, 4-Me-Ph	**18**
	R^3 = 2-NO_2, 4-Cl-Ph	**19**
	R^3 = 3-CF_3-Ph	**20**
	R^3 = 4-NO_2-Ph	**21**
	R^3 = 4-OMe-Ph	**22**
	R^3 = 4-Me-Ph	**23**
X=O, R^1=R^2 = OEt	R^3 = Ph	**24**
	R^3 = 2,4-diCl-Ph	**25**
	R^3 = 4-NO_2-Ph	**26**
	R^3 = 4-Me-Ph	**27**
X=O, R^1 = H, R^2 = OMe	R^3 = Ph	**28**
	R^3 = 2-NO_2, 4-Cl-Ph	**29**
X=NH, R^1=R^2 = OMe	R^3 = 3-CF_3-Ph	**30**
	R^3 = 2-NO_2, 4-Me-Ph	**31**
	R^3 = 2-NO_2, 4-Cl-Ph	**32**

[a]Reagents: i) PyBOP, TEA, r.t., CH_2Cl_2

CHARTS

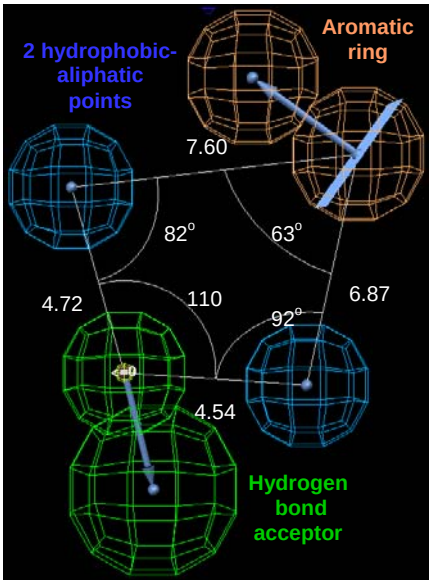

Chart 1. Pharmacophore features and their angles and distances relation (Å).

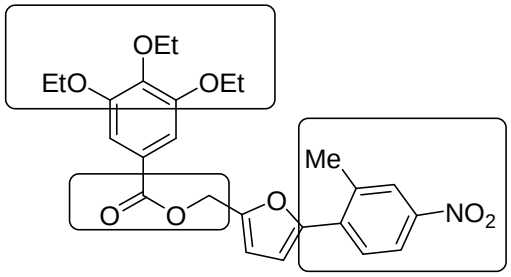

Chart 2. Selected lead compound **1** for further optimization and areas where modifications have been done.

TABLE OF CONTENTS GRAPHIC